First-principles design and subsequent synthesis of a material to search for the permanent electric dipole moment of the electron

K. Z. Rushchanskii,[1] S. Kamba,[2] V. Goian,[2] P. Vaněk,[2] M. Savinov,[2] J. Prokleška,[3] D. Nuzhnyy,[2]
K. Knížek,[2] F. Laufek,[4] S. Eckel,[5] S. K. Lamoreaux,[5] A. O. Sushkov,[5] M. Ležaić,[1] and N. A. Spaldin[6]

[1]*Institut für Festkörperforschung, Forschungszentrum Jülich GmbH 52425 Jülich and JARA-FIT, Germany*
[2]*Institute of Physics ASCR, Na Slovance 2, 182 21 Prague 8, Czech Republic*
[3]*Charles University, Faculty of Mathematics and Physics,*
Department of Condensed Matter Physics, Ke Karlovu 5, 121 16 Prague 2, Czech Republic
[4]*Czech Geological Survey, Geologická 6, 152 00 Prague 5, Czech Republic*
[5]*Yale University, Department of Physics, P.O. Box 208120, New Haven, CT 06520-8120*
[6]*Materials Department, University of California, Santa Barbara, CA 93106-5050, USA*
(Dated: October 24, 2018)

We describe the first-principles design and subsequent synthesis of a new material with the specific functionalities required for a solid-state-based search for the permanent electric dipole moment of the electron. We show computationally that perovskite-structure europium barium titanate should exhibit the required large and pressure-dependent ferroelectric polarization, local magnetic moments, and absence of magnetic ordering at liquid helium temperature. Subsequent synthesis and characterization of $Eu_{0.5}Ba_{0.5}TiO_3$ ceramics confirm the predicted desirable properties.

The Standard Model of particle physics incorporates the breaking of the discrete symmetries of parity (P) and the combined charge conjugation and parity (CP). It is thought however, that the CP-violation within the framework of the Standard Model is insufficient to explain the observed matter-antimatter asymmetry of the Universe[1], therefore a so far unknown source of CP-violation likely exists in nature. The existence of a non-zero permanent electric dipole moment (EDM) of a particle, such as an electron, neutron, or atom, would violate time reversal (T) symmetry (Fig. 1) and therefore imply CP-violation through the CPT theorem[2]. In the Standard Model these EDMs are strongly suppressed, the theoretical predictions lying many orders of magnitude below the current experimental limits. However, many theories beyond the Standard Model, such as supersymmetry, contain a number of CP-violating phases that lead to EDM predictions within experimental reach[3]. Searching for EDMs therefore constitutes a background-free method of probing the CP-violating physics beyond the
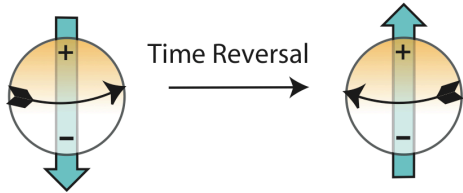

FIG. 1: Illustration that an electron with an electric dipole moment violates time-reversal symmetry. Both the electric dipole moment (+ and - symbols; orange shading) and magnetic moment (blue arrow) of the electron lie along the same axis as the electron spin (black arrow). The operation of time reversal reverses the magnetic moment but does not affect the electric dipole moment; therefore an electron with a non-zero electric dipole moment violates time-reversal symmetry.
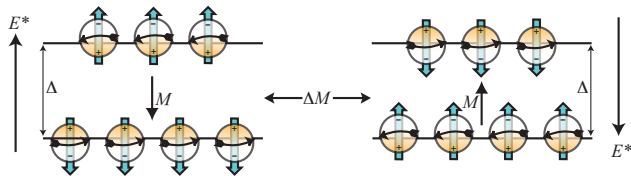
Standard Model.

A number of experimental EDM searches are currently under way or are being developed – systems studied in these experiments include diatomic molecules[4,5], diamagnetic atoms[6–8], molecular ions[9], cold atoms[10], neutrons[11], liquids[12], and solids[13,14] – with one of the most promising novel techniques being electric-field-correlated magnetization measurements in solids[15–17]. This technique rests on the fact that, since spin is the only intrinsic vector associated with the electron, a non-vanishing electron EDM is either parallel or antiparallel to its spin and hence its magnetic moment. As a result, when an electric field, which lifts the degeneracy between electrons with EDMs parallel and antiparallel to it, is applied to a sample, the associated imbalance of electron populations generates a magnetization (Fig. 2). The orientation of the magnetization is reversed when the electric field direction is switched; in our proposed experiment we will monitor this change in sample magnetization using a SQUID magnetometer[18,19]. Such *magnetoelectric responses* in materials with permanent *macroscopic* magnetizations and polarizations are of great current interest in the materials science community because of their potential for enabling novel devices that tune and control magnetism using electric fields[20].

Since the experiment aims to detect the intrinsic magnetoelectric response associated with the tiny electric dipole moment of the electron, the design constraints on the material are stringent. First, the solid must contain magnetic ions with unpaired spins, since the equal and opposite spins of paired electrons have corresponding equal and opposite EDMs and contribute no effect. Second, it must be engineered such that the *conventional* linear magnetoelectric tensor is zero; our approach to achieving this is to use a paramagnet in which the conventional effect is forbidden by time-reversal symmetry[21]. To reach the required sensitivity, a high atomic density

hence of the effective electric field, with a moderate applied electric field. Finally, the experiment will be performed inside liquid helium, so the material properties described above must persist at low temperature. A detailed derivation of the dependence of the sensitivity on the material parameters is given in Ref.[19]. Note that conventional impurities such as defects or domain walls are not detrimental to the experiment since they do not violate time-reversal symmetry. In summary, the following material specifications will allow a sensitive EDM search to be mounted: (i) The material should be ferroelectric, with a large electric polarization, and switchable at liquid He temperature. (ii) There should be a high concentration of ions with local magnetic moments that remain paramagnetic at liquid He temperature; both long-range order and freezing into a glassy state must be avoided. (iii) The local environment at each magnetic ion should be strongly modified by the ferroelectric switching, and (iv) the sample should be macroscopic. With these material properties, and optimal SQUID noise levels, the projected experimental sensitivity is 10^{-28} e.cm after ten days of averaging[19].

No known materials meet all the requirements. Indeed the contra-indication between ferroelectricity and magnetism has been studied extensively over the last decade in the context of multiferroics[23], where the goal has been to achieve simultaneous ferroelectric and ferromagnetic ordering at high temperature. In spite of extensive efforts, a room temperature multiferroic with large and robust ferroelectricity and magnetization at room temperature remains elusive. While the low temperature constraints imposed here seem at first sight more straightforward, avoiding any magnetic ordering at low temperature, while retaining a high concentration of magnetic ions poses a similarly demanding challenge. In addition the problem of ferroelectric switchability at low temperature is challenging, since coercivities tend to increase as temperature is lowered[24].

We proceed by proposing a trial compound and calculating its properties using density functional theory to determine whether an experimental synthesis should be motivated. We choose an alloy of europium titanate, $EuTiO_3$ and barium titanate, $BaTiO_3$, with motivation as follows: To incorporate magnetism we require unfilled orbital manifolds of localized electrons; to avoid magnetic ordering the exchange interactions should be small. Therefore the tightly bound $4f$ electrons are likely to be the best choice. For conventional ferroelectricity we require transition metal ions with empty d orbitals to allow for good hybridization with coordinating anions on off-centering[25]. (Note that while here we use a conventional ferroelectric mechanism, many alternative routes to ferroelectricity that are compatible with magnetism – and which could form a basis for future explorations – have been recently identified; for a review see Ref. 26). Both $EuTiO_3$ and $BaTiO_3$ form in the ABO_3 perovskite structure, with divalent Eu^{2+} or Ba^{2+} on the A site, and formally d^0 Ti^{4+} on the B site. $BaTiO_3$ is a prototypical

FIG. 2: Schematic of the physics underlying the experiment to search for the electron EDM. The energy of electrons with EDMs parallel to the effective electric field E^* is lower than that for electrons with anti-parallel EDMs by an amount $\Delta = E^* \cdot d_e$. As a result there is a population imbalance (exaggerated for clarity in the figure), and, since the magnetic moments are aligned along the EDM directions, a corresponding net magnetization, M. When the electric field is reversed there is a magnetization reversal, ΔM, which can be detected using a sensitive magnetometer.

of magnetic ions ($n \approx 10^{22}$ cm^{-3}) is needed, and these magnetic ions must reside at sites with broken inversion symmetry. The energy splitting Δ shown in Fig. 2 is proportional to the product of the effective electric field experienced by the electron, E^*, and its electric dipole moment, d_e. The effective electric field, which is equal to the electric field one would have to apply to a free electron to obtain the same energy splitting, is in turn determined by the displacement of the magnetic ion from the center of its coordination polyhedron; for a detailed derivation see Ref.[22]. For example, in $Eu_{0.5}Ba_{0.5}TiO_3$ ceramics (see below) with ~ 1 $\mu C/cm^2$ remanent polarization, the mean displacement of the Eu^{2+} ion with respect to its oxygen cage is 0.01 Å and this results in an effective electric field of ~ 10 MV/cm, even when no external electric field is applied. We choose a ferroelectric so that it is possible to reverse the direction of the ionic displacements, and

ferroelectric with a large room temperature polarization of 25 $\mu C/cm^2$.[27] In the cubic paraelectric phase its lattice constant is 3.996 Å[28]. The Ba^{2+} ion has an inert gas electron configuration and hence zero magnetic moment.

The lattice parameter of $EuTiO_3$ is 3.905 Å[29], notably smaller than that of $BaTiO_3$. It is not ferroelectric, but has a large dielectric constant ($\epsilon \approx 400$) at low temperature, indicative of proximity to a ferroelectric phase transition; indeed it has recently been reported to be a quantum paraelectric[29,30]. First-principles electronic structure calculations have shown that ferroelectricity should be induced along the elongation direction by either compressive or tensile strain[31]. The Eu^{2+} ion has seven unpaired localized $4f$ electrons resulting in a large spin magnetization of 7 μ_B, and $EuTiO_3$ is an antiferromagnet with G-type ordering at a low Néel temperature of ~ 5.3 K[32,33]. (Independently of the study presented here, $EuTiO_3$ is of considerable current interest because its dielectric response is strongly affected by the magnetic ordering[29,30] and because of its unusual third order magnetoelectric response[34]. These behaviors indicate coupling between the magnetic and dielectric orders caused by sensitivity of the polar soft mode to the magnetic ordering[31,35].)

Our hypothesis is that by alloying Ba on the A-site of $EuTiO_3$, the magnetic ordering temperature will be suppressed through dilution, and the tendency to ferroelectricity will be increased through the expansion of the lattice constant. Our hope is to identify an alloying range in which the magnetic ordering temperature is sufficiently low while the ferroelectric polarization and the concentration of magnetic ions remain sufficiently large. In addition, we expect that the polarization will be sensitive to the lattice constant, allowing its magnitude and consequently the coercivity, to be reduced with pressure.

I. FIRST-PRINCIPLES CALCULATIONS

Taking the 50/50 (Eu,Ba)TiO$_3$ ordered alloy as our starting point (Fig. 3 inset), we next calculate its properties using first-principles. For details of the computations see the Methods section.

We began by calculating the phonon dispersion for the high symmetry, cubic perovskite reference structure at a lattice constant of 3.95 Å (chosen, somewhat arbitrarily, for this first step because it is the average of the experimental $BaTiO_3$ and $EuTiO_3$ lattice constants), with the magnetic spins aligned ferromagnetically; our results are shown in Fig. 3, plotted along the high symmetry lines of the Brillouin zone. Importantly we find a polar Γ-point instability with an imaginary frequency of $103i$ cm^{-1} which is dominated by relative oxygen – Ti/Eu displacements (the eigenmode displacements for Eu, Ba, Ti, O$_\parallel$ and O$_\perp$ are 0.234, -0.059, 0.394, -0.360 and -0.303 respectively); such polar instabilities are indicative of a tendency to ferroelectricity. The zone boundary rotational instabilities that often occur in perovskite oxides
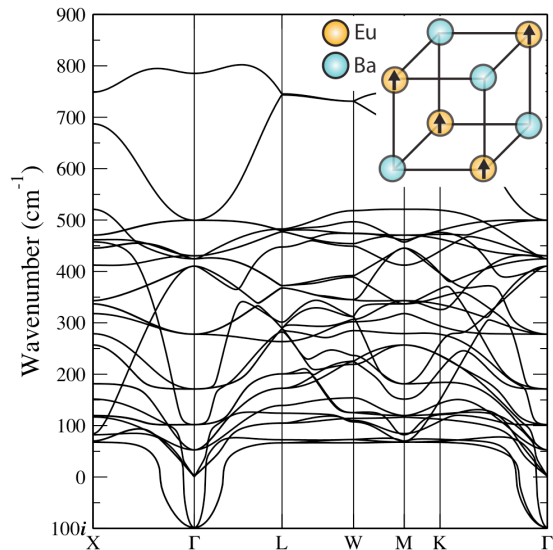

FIG. 3: Calculated phonon dispersion of ferromagnetic $Eu_{0.5}Ba_{0.5}TiO_3$ in its high symmetry reference structure with pseudo-cubic lattice constant $a_0 = 3.95$ Å. The imaginary frequency polar phonon at Γ indicates a structural instability to a ferroelectric phase. The inset shows the supercell of the ferromagnetic $Eu_{0.5}Ba_{0.5}TiO_3$ ordered alloy used in our calculations. The Ti and O ions are omitted for clarity; arrows represent the Eu magnetic moments.

and lead to non-polar, antiferrodistortive ground states are notably absent (in fact the flat bands at ~ 60 cm^{-1} are stable rotational vibrations). Interestingly we find that the Eu ions have a significant amplitude in the soft-mode eigenvector, in contrast to the Ba ions both here and in the parent $BaTiO_3$.

Next we performed a structural optimization of both the unit cell shape and the ionic positions of our $Eu_{0.5}Ba_{0.5}TiO_3$ alloy with the total volume constrained to that of the ideal cubic structure studied above (3.95^3 Å^3 per formula unit). Our main finding is that the $Eu_{0.5}Ba_{0.5}TiO_3$ alloy is polar with large relative displacements of oxygen and both Ti and Eu relative to the high symmetry reference structure. Using the Berry phase method we obtain a ferroelectric polarization value of $P = 23$ $\mu C/cm^2$. Our calculated ground state is orthorhombic with the polarization oriented along a [011] direction and lattice parameters $a = 3.94$ Å, $b = 5.60$ Å and $c = 5.59$ Å. As expected from our analysis of the soft mode, the calculated ground state is characterized by large oxygen – Ti/Eu displacements, and the absence of rotations or tilts of the oxygen octahedra. Importantly, the large Eu amplitude in the soft mode manifests as a large off-centering of the Eu from the center of its oxygen coordination polyhedron in the ground state structure. The origin of the large Eu displacement lies in its small ionic radius compared with that of divalent Ba^{2+}:

The large coordination cage around the Eu ion which is imposed by the large lattice constant of the alloy results in under-bonding of the Eu that can be relieved by off-centering. Indeed, we find that in calculations for fully relaxed single phase $EuTiO_3$, the oxygen octahedra tilt to reduce the volume of the A site in a similar manner to those known to occur in $SrTiO_3$, in which the A cation size is almost identical. This Eu off-centering is desirable for the EDM experiment because the change in local environment at the magnetic ions on ferroelectric switching determines the sensitivity of the EDM measurement.

volume (Å^3)	P ($\mu C/cm^2$)
61.63 (constrained)	23
62.30 (experimental)	28
64.63 (relaxed)	44

TABLE I: Calculated ferroelectric polarizations, P, of $Eu_{0.5}Ba_{0.5}TiO_3$ at three different volumes.

We note that the magnitude of the polarization is strongly dependent on the volume used in the calculation (Table I). At the experimental volume (reported in the next section), which is only slightly larger than our constrained volume of 3.95^3 Å^3, we obtain a polarization of 28 $\mu C/cm^2$. At full relaxation, where we find a larger volume close to that of $BaTiO_3$, we obtain a polarization of 44 $\mu C/cm^2$, almost certainly a substantial over-estimate. This volume dependence suggests that the use of pressure to reduce the lattice parameters and suppress the ferroelectric polarization could be a viable tool for reducing the coercivity at low temperatures. Indeed our computations show that, at a pressure corresponding to 2.8 GPa applied to the experimental volume the theoretical structure is cubic, with both the polarization and coercive field reduced to zero.

Finally, to investigate the likelihood of magnetic ordering, we calculated the relative energies of the ferromagnetic state discussed above and of two antiferromagnetic arrangements: planes of ferromagnetically ordered spins coupled antiferromagnetically along either the pseudo-cubic z axis or the x or y axes. (Note that these are degenerate in the high-symmetry cubic structure). For each magnetic arrangement we re-relaxed the lattice parameters and atomic positions. As expected for the highly localized Eu $4f$ electrons on their diluted sublattice, the energy differences between the different configurations are small – around 1 meV per 40 atom supercell – suggesting an absence of magnetic ordering down to low temperatures. While our calculations find the ferromagnetic state to be the lowest energy, this is likely a consequence of our A-site ordering and should not lead us to anticipate ferromagnetism at low temperature (Note that, after completing our study, we found a report of an early effort to synthesize $(Eu,Ba)TiO_3$[36] in which a large magnetization, attributed to A-site ordering and ferromagnetism, was reported. A-site ordering is now known to be difficult to achieve in perovskite-structure oxides, however,

and we find no evidence of it in our samples. Moreover the earlier work determined a tetragonal crystal structure in contrast to our refined orthorhombic structure.)

In summary, our predicted properties of the $(Eu,Ba)TiO_3$ alloy – large ferroelectric polarization, reducible with pressure, with large Eu displacements, and strongly suppressed magnetic ordering – meet the criteria for the electron electric dipole moment search and motivate the synthesis and characterization of the compound, described next.

II. SYNTHESIS

$Eu_{0.5}Ba_{0.5}TiO_3$ was synthesized by solid-state reaction using mechanochemical activation before calcination. For details see the Methods section. The density of the sintered pellets was 86-88% of the theoretical density. X-ray diffraction at room temperature revealed the cubic perovskite $Pm\bar{3}m$ structure with a=3.9642(1) Å. At 100 K we obtain an orthorhombic ground state with space group $Amm2$, in agreement with the GGA+U prediction, and lattice parameters 3.9563(1), 5.6069(2) and 5.5998(2) Å.

III. CHARACTERIZATION

The final step in our study is the characterization of the samples, to check that the measured properties are indeed the same as those that we predicted and desired. Figure 4 shows the temperature dependence of the complex permittivity between 1 Hz and 1 MHz, measured using an impedance analyzer ALPHA-AN (Novocontrol). The low-frequency data below 100 kHz are affected above 150 K by a small defect-induced conductivity and related Maxwell-Wagner polarization; the high-frequency data clearly show a maximum in the permittivity near T_c=213 K indicating the ferroelectric phase transition. Two regions of dielectric dispersion – near 100 K and below 75 K – are seen in $\tan\delta(T)$; these could originate from oxygen defects or from ferroelectric domain wall motion.

Measurement of the polarization was adversely affected by the sample conductivity above 150 K, but at lower temperatures good quality ferroelectric hysteresis loops were obtained (Fig. 4, inset). At 135 K we obtain a saturation polarization of $\sim$8 $\mu C/cm^2$. The deviation from the predicted value could be the result of incomplete saturation as well as the strong volume dependence of the polarization combined with the well-known inaccuracies in GGA+U volumes. As expected, at lower temperatures the coercive field strongly increases, and only partial polarization switching was possible even with an applied electric field of 18 kV/cm (at higher electric field dielectric breakdown was imminent). The partial switching is responsible for the apparent decrease in saturation polarization below 40 K.

Time-domain THz transmission and infrared reflectivity spectra (not shown here) reveal a softening of the
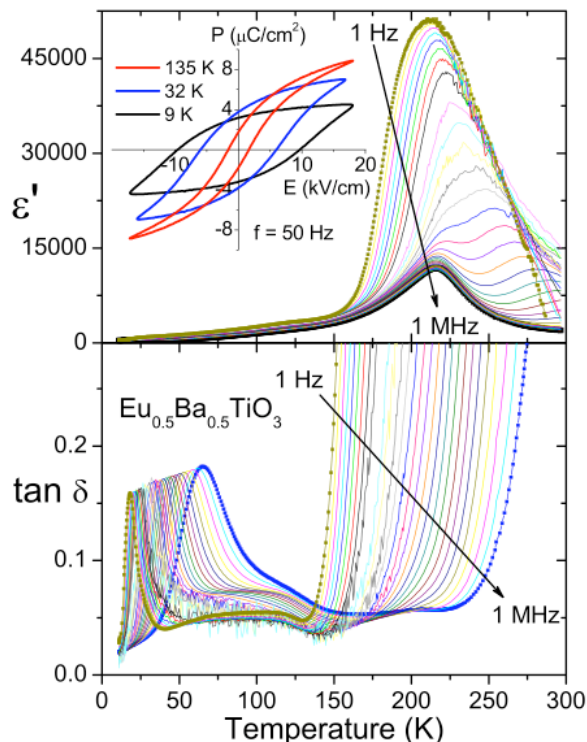
FIG. 4: Temperature dependence of permittivity and dielectric loss in $Eu_{0.5}Ba_{0.5}TiO_3$ ceramics. The arrows indicate the direction of increasing frequency and the colors are for clarity to assist the eye in distinguishing the lines. The inset shows ferroelectric hysteresis loops measured at three temperatures and 50 Hz.

polar phonon from $\sim 40\,cm^{-1}$ at 300 K to $\sim 15\,cm^{-1}$ at T_c, and then its splitting into two components in the ferroelectric phase. Both components harden on cooling below T_c, with the lower frequency component remaining below $20\,cm^{-1}$ down to 10 K, and the higher-frequency branch saturating near $70\,cm^{-1}$ at 10 K. This behavior is reminiscent of the soft-mode behavior in $BaTiO_3$[37]. However, when we extract the contribution to the static permittivity that comes from the polar phonon, we find that it is considerably smaller than our measured value (Fig. 4) indicating an additional contribution to the dielectric relaxation. Our observations suggest that the phase transition is primarily soft-mode driven, but also exhibits some order-disorder character.

Finally, we measured the magnetic susceptibility χ at various static magnetic fields as a function of temperature down to 0.4 K. (For details see the Methods section.) Our results are shown in Fig. 5. $\chi(T)$ peaks at $T \sim 1.9\,K$ indicating an absence of magnetic ordering above this temperature. The $\chi(T)$ data up to 300 K show Curie-Weiss behavior $\chi(T) = \frac{C}{T+\theta}$ with θ=-1.63 K and $C = 0.017$ emuK/(gOe). The peak in susceptibility at 1.9K is frequency independent and not influenced by zero field heating measurements after field cooling, confirming antiferromagnetic order below $T_N = 1.9\,K$.
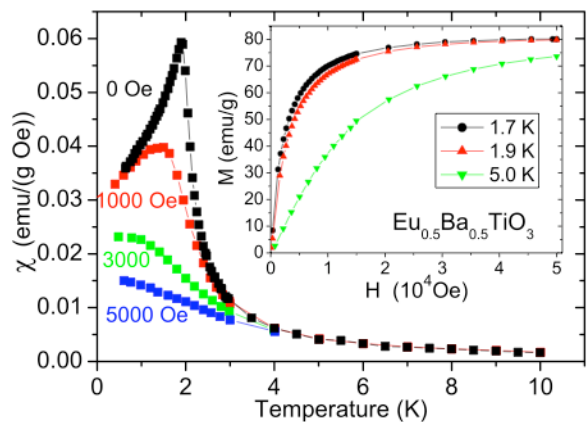

FIG. 5: Temperature dependence of ac magnetic susceptibility, χ, at various static magnetic fields and frequency of 214 Hz. Inset shows magnetization curves at various temperatures. We note that no hysteresis in magnetization was observed.

As in pure $EuTiO_3$, the $\chi(T)$ peak is suppressed by a static external magnetic field, indicating stabilization of the paramagnetic phase[29]. Magnetization curves (Fig. 5 inset) show saturation above 2×10^4 Oe at temperatures below T_N and slower saturation at 5 K. No open magnetic hysteresis loops were observed.

In summary, we have designed a new material – $Eu_{0.5}Ba_{0.5}TiO_3$ – with the properties required to enable a measurement of the EDM to a higher accuracy than can currently be realized. Subsequent synthesis of $Eu_{0.5}Ba_{0.5}TiO_3$ ceramics confirmed their desirable ferroelectric polarization and absence of magnetic ordering above 1.9 K. The search for the permanent dipole moment of the electron using $Eu_{0.5}Ba_{0.5}TiO_3$ is now underway. Initial measurements have already achieved an EDM upper limit of 5×10^{-23} e.cm, which is within a factor of 10 of the current record with a solid-state-based EDM search[13]. We are currently studying a number of systematic effects that may mask the EDM signal. The primary error originates from ferroelectric hysteresis-induced heating of the samples during polarization reversal. This heating gives rise to a change in magnetic susceptibility, which, in a non-zero external magnetic field, leads to an undesirable sample magnetization response. We are working to control the absolute magnetic field at the location of the samples to the 0.1 μG level. Our projected sensitivity of 10^{-28} e.cm should then be achievable.

V. AUTHOR CONTRIBUTIONS

SKL supervised the EDM measurement effort at Yale. AOS and SE performed the analysis and made preliminary measurements, showing that these materials could be useful in an EDM experiment. ML and NAS selected $(Eu,Ba)TiO_3$ as the candidate material according to the experimental requirements and supervised the ab-initio calculations. KZR performed the ab-initio calculations. ML, NAS and KZR analysed the ab-initio results and wrote the theoretical component of the paper. Ceramics were prepared by PV. Crystal structure was determined by KK and FL. Dielectric measurements were performed by MS. JP investigated magnetic properties of ceramics. VG performed infrared reflectivity studies. DN investigated THz spectra. SK coordinated all experimental studies and wrote the synthesis and characterization part of manuscript. NAS coordinated the preparation of the manuscript.

VI. METHODS

A. Computational details

We performed first-principles density-functional calculations within the spin-polarized generalized gradient approximation (GGA)[38]. The strong on-site correlations of the Eu $4f$ electrons were treated using the GGA+U method[39] with the double counting treated within the Dudarev approach[40] and parameters $U = 5.7$ eV and $J = 1.0$ eV. For structural relaxation and lattice dynamics we used the Vienna *Ab Initio* Simulation Package (VASP)[41] with the default projector augmented-wave (PAW) potentials[42] (valence-electron configurations Eu:

$5s^25p^64f^76s^2$, Ba: $5s^25p^66s^2$, Ti: $3s^23p^63d^24s^2$ and O: $2s^22p^4$.) Spin-orbit interaction was not included.

The 50/50 $(Eu,Ba)TiO_3$ alloy was represented by an ordered A-site structure with the Eu and Ba ions alternating in a checkerboard pattern (Fig. 3, inset). Structural relaxations and total energy calculations were performed for a 40-atom supercell (consisting of two 5-atom perovskite unit cells in each cartesian direction) using a $4 \times 4 \times 4$ Γ-centered k-point mesh and a plane-wave cutoff of 500 eV. Ferroelectric polarizations and Born effective charges were calculated using the Berry phase method[43]. Lattice instabilities were investigated in the frozen-phonon scheme[44,45] for an 80 atom supercell using a Γ-centered $2 \times 2 \times 2$ k-point mesh and 0.0056 Å atomic displacements to extract the Hellman-Feynman forces.

B. Synthesis

Eu_2O_3, TiO_2 (anatase) and $BaTiO_3$ powders (all from Sigma-Aldrich) were mixed in stoichiometric ratio then milled intensively in a planetary ball micro mill Fritsch Pulverisette 7 for 120 min. in a dry environment followed by 20 min. in suspension with n-heptane. ZrO_2 grinding bowls (25 ml) and balls (12 mm diameter, acceleration 14 g) were used. The suspension was dried under an IR lamp and the dried powder was pressed in a uniaxial press (330 MPa, 3 min.) into 13 mm diameter pellets. The pellets were calcined in pure H_2 atmosphere at 1200 ℃ for 24 hr (to reduce Eu^{3+} to Eu^{2+}), then milled and pressed by the same procedure as above and sintered at 1300 ℃ for 24 hr in $Ar + 10\% H_2$ atmosphere. Note that pure H_2 can not be used for sintering without adversely increasing the conductivity of the sample.

C. Characterization

Magnetic susceptibility was measured using a Quantum Design PPMS9 and a He^3 insert equipped with a home-made induction coil that allows measurement of ac magnetic susceptibility, χ from 0.1 to 214 Hz.

---

[1] Trodden, M. Electroweak baryogenesis. *Rev. Mod. Phys.* **71**, 1463–1500 (1999).

[2] Khriplovich, I. B. & Lamoreaux, S. K. *CP violation without strangeness* (Springer, Berlin, 1997).

[3] Bernreuther, W. & Suzuki, M. The electric dipole moment of the electron. *Rev. Mod. Phys.* **63**, 313–340 (1991).

[4] Hudson, J. J., Sauer, B. E., Tarbutt, M. R. & Hinds, E. A. Measurement of the electron electric dipole moment using YbF molecules. *Phys. Rev. Lett.* **89**, 023003 (2002).

[5] Kawall, D., Bay, F., Bickman, S., Jiang, Y. & DeMille, D. Precision Zeeman-Stark spectroscopy of the metastable a(1)[$^3\sigma^+$] state of PbO. *Phys. Rev. Lett.* **92**, 133007 (2004).

[6] Griffith, W. C. *et al.* Improved limit on the permanent electric dipole moment of ^{199}Hg. *Phys. Rev. Lett.* **102**, 101601 (2009).

[7] Guest, J. R. *et al.* Laser trapping of ^{225}Ra and ^{226}Ra with repumping by Room-Temperature blackbody radiation. *Phys. Rev. Lett.* **98**, 093001 (2007).

[8] Tardiff, E. R. *et al.* Polarization and relaxation of ^{209}Rn. *Nuclear Instruments and Methods in Physics Research Section A: Accelerators, Spectrometers, Detectors and Associated Equipment* **579**, 472–475 (2007).

[9] Stutz, R. P. & Cornell, E. A. Search for the electron EDM using trapped molecular ions. *Bull. Am. Phys. Soc.* **89**, 76 (2004).

[10] Weiss, D. S., Fang, F. & Chen, J. Measuring the eletric dipole moment of Cs and Rb in an optical lattice. *Bull. Am. Phys. Soc.* **APR03**, J1.008 (2003).

[11] Baker, C. A. *et al.* Improved experimental limit on the electric dipole moment of the neutron. *Phys. Rev. Lett.* **97**, 131801 (2006).

[12] Ledbetter, M. P., Savukov, I. M. & Romalis, M. V. Nonlinear amplification of small spin precession using Long-Range dipolar interactions. *Phys. Rev. Lett.* **94**, 060801 (2005).

[13] Heidenreich, B. J. *et al.* Limit on the electron electric dipole moment in Gadolinium-Iron garnet. *Phys. Rev. Lett.* **95**, 253004 (2005).

[14] Bouchard, L. S., Sushkov, A. O., Budker, D., Ford, J. J. & Lipton, A. S. Nuclear-spin relaxation of ^{207}Pb in ferroelectric powders. *Phys. Rev. A* **77**, 022102 (2008).

[15] Shapiro, F. L. Electric dipole moments of elementary particles. *Soviet physics, Uspekhi* **11**, 345 (1968).

[16] Lamoreaux, S. K. Solid-state systems for the electron electric dipole moment and other fundamental measurements. *Phys. Rev. A* **66**, 022109 (2002).

[17] Budker, D., Lamoreaux, S. K., Sushkov, A. O. & Sushkov, O. P. Sensitivity of condensed-matter P- and T-violation experiments. *Phys. Rev. A* **73**, 022107 (2006).

[18] Sushkov, A. O., Eckel, S. & Lamoreaux, S. K. Prospects for a new search for the electron electric-dipole moment in solid gadolinium-iron-garnet ceramics. *Phys. Rev. A* **79**, 022118–8 (2009).

[19] Sushkov, A. O., Eckel, S. & Lamoreaux, S. K. The prospects for an electron electric dipole moment search with ferroelectric (Eu,Ba)TiO$_3$ ceramics. *Phys. Rev. A* **81**, 022104 (2010).

[20] Spaldin, N. A. & Ramesh, R. Electric-field control of magnetism in complex oxide thin films. *MRS Bulletin* **33**, 1047–1050 (2008).

[21] Fiebig, M. Revival of the magnetoelectric effect. *J. Phys. D: Appl. Phys.* **38**, R1–R30 (2005).

[22] Mukhamedjanov, T. N., Dzuba, V. A. & Sushkov, O. P. Enhancement of the electron electric dipole moment in gadolinium garnets. *Phys. Rev. A* **68**, 042103 (2003).

[23] Hill, N. A. Why are there so few magnetic ferroelectrics? *J. Phys. Chem. B* **104**, 6694–6709 (2000).

[24] Merz, W. J. The dielectric properties of BaTiO$_3$ at low temperatures. *Phys. Rev.* **81**, 1064–1065 (1951).

[25] Rondinelli, J. M., Eidelson, A. S. & Spaldin, N. A. Non-d^0 mn-driven ferroelectricity in antiferromagnetic BaMnO$_3$. *Physical Review B (Condensed Matter and Materials Physics)* **79**, 205119 (2009).

[26] Ramesh, R. & Spaldin, N. A. Multiferroics: Progress and prospects in thin films. *Nature Materials* **6**, 21–29 (2007).

[27] Wemple, S., Jr., M. D. & Camlibel, I. Dielectric and optical properties of melt-grown BaTiO$_3$. *J. Phys. Chem. Sol.* **29**, 1797–1803 (1968).

[28] Miyake, S. & Ueda, R. On phase transformation of BaTiO$_3$. *J. Phys. Soc. Jpn.* **2**, 93–97 (1947).

[29] Katsufuji, T. & Takagi, H. Coupling between magnetism and dielectric properties in quantum paraelectric EuTiO$_3$. *Phys. Rev. B* **64**, 054415 (2001).

[30] Kamba, S. *et al.* Magnetodielectric effect and optic soft mode behaviour in quantum paraelectric EuTiO$_3$ ceramics. *Europhys. Lett.* **80**, 27002 (2007).

[31] Fennie, C. J. & Rabe, K. M. Magnetic and electric phase control in epitaxial EuTiO$_3$ from first principles. *Phys. Rev. Lett.* **97**, 267602 (2006).

[32] McGuire, T. R., Shafer, M. W., Joenk, R. J., Alperin, H. A. & Pickart, S. J. Magnetic structure of EuTiO$_3$. *J. Appl. Phys.* **37**, 981–982 (1966).

[33] Chien, C.-L., DeBenedetti, S. & Barros, F. D. S. Magnetic properties of EuTiO$_3$, Eu$_2$TiO$_4$, and Eu$_3$Ti$_2$O$_7$. *Phys. Rev. B* **10**, 3913–3922 (1974).

[34] Shvartsman, V. V., Borisov, P., Kleemann, W., Kamba, S. & Katsufuji, T. Large off-diagonal magnetoelectric coupling in the quantum paraelectric antiferromagnet EuTiO$_3$. *Phys. Rev. B* **81**, 064426 (2010).

[35] Goian, V. *et al.* Polar phonon mixing in magnetoelectric EuTiO$_3$. *Eur. Phys. J. B* **71**, 429–433 (2009).

[36] Janes, D. L., Bodnar, R. E. & Taylor, A. L. Europium barium titanate – a magnetic ferroelectric compound. *J. Appl. Phys.* **49**, 1452–1454 (1978).

[37] Hlinka, J. *et al.* Coexistence of the phonon and relaxation soft mode in the terahertz dielectric response of tetragonal BaTiO$_3$. *Phys. Rev. Lett.* **101**, 167402 (2008).

[38] Perdew, J. P., Burke, K. & Ernzerhof, M. Generalized gradient approximation made simple. *Phys. Rev. Lett.* **77**, 3865–3868 (1996).

[39] Anisimov, V. I., Aryasetiawan, F. & Liechtenstein, A. I. First-principles calculations of the electronic structure and spectra of strongly correlated systems: the LDA+U method. *J. Phys.: Condens. Matter* **9**, 767–808 (1997).

[40] Dudarev, S. L., Botton, G. A., Savrasov, S. Y., Humphreys, C. J. & Sutton, A. P. Electron-energy-loss spectra and the structural stability of nickel oxide: An LSDA+U study. *Phys. Rev. B* **57**, 1505–1509 (1998).

[41] Kresse, G. & Furthmüller, J. Efficient iterative schemes for ab initio total-energy calculations using a plane-wave basis set. *Phys. Rev. B* **54**, 11169–11186 (1996).

[42] Blöchl, P. E. Projector augmented-wave method. *Phys. Rev. B* **50**, 17953–17979 (1994).

[43] King-Smith, R. D. & Vanderbilt, D. Theory of polarization of crystalline solids. *Phys. Rev. B* **47**, 1651–1654 (1993).

[44] Kunc, K. & Martin, R. M. Ab initio force constants of GaAs: A new approach to calculation of phonons and dielectric properties. *Phys. Rev. Lett.* **48**, 406–409 (1982).

[45] Alfe, D. PHON: A program to calculate phonons using the small displacement method. *Comp. Phys. Comm.* **180**, 2622–2633 (2009).